PAPER

Cite this: *RSC Adv.*, 2024, **14**, 15261

Vanadium pentoxide interfacial layer enables high performance all-solid-state thin film batteries†

Shiping Ma,‡[a] Kaiyuan Wei,‡[b] Yu Zhao, [ID] [a] Jinxu Qiu, [ID] [a] Rongrui Xu,[a] Hongliang Li,[a] Hui Zhang*[c] and Yanhua Cui [ID] *[a]

Lithium cobalt oxide (LiCoO$_2$) is considered as one of the promising building blocks that can be used to fabricate all-solid-state thin film batteries (TFBs) because of its easy accessibility, high working voltage, and high energy density. However, the slow interfacial dynamics between LiCoO$_2$ and LiPON in these TFBs results in undesirable side reactions and severe degradation of cycling and rate performance. Herein, amorphous vanadium pentoxide (V$_2$O$_5$) film was employed as the interfacial layer of a cathode–electrolyte solid–solid interface to fabricate all-solid-state TFBs using a magnetron sputtering method. The V$_2$O$_5$ thin film layer assisted in the construction of an ion transport network at the cathode/electrolyte interface, thus reducing the electrochemical redox polarization potential. The V$_2$O$_5$ interfacial layer also effectively suppressed the side reactions between LiCoO$_2$ and LiPON. In addition, the interfacial resistance of TFBs was significantly decreased by optimizing the thickness of the interfacial modification layer. Compared to TFBs without the V$_2$O$_5$ layer, TFBs based on LiCoO$_2$/V$_2$O$_5$/LiPON/Li with a 5 nm thin V$_2$O$_5$ interface modification layer exhibited a much smaller charge transfer impedance (R_{ct}) value, significantly improved discharge specific capacity, and superior cycling and rate performance. The discharge capacity remained at 75.6% of its initial value after 1000 cycles at a current density of 100 μA cm^{-2}. This was mainly attributed to the enhanced lithium ion transport kinetics and the suppression of severe side reactions at the cathode–electrolyte interface in TFBs based on LiCoO$_2$/V$_2$O$_5$/LiPON/Li with a 5 nm V$_2$O$_5$ thin layer.

1. Introduction

With the rapid development of equipment intelligence and miniaturization, there is an urgent need for energy sources that can be integrated with microdevices.[1] The all-solid-state lithium-ion thin film battery (TFB) has been regarded as a potential and ideal alternative due to its advantages of ultra-thin device size of several hundred micrometers (including packaging layers), excellent environmental adaptability, long cycle life, and superior storage life.[1] Microscale TFBs that are flexible and three-dimensional are promising candidates for the above applications because of their safety and flexible structure.[1,2]

[a]Laboratory of Electrochemical Power Sources, Institute of Electronic Engineering, China Academy of Engineering Physics, Mianyang, Sichuan 621000, P. R. China. E-mail: cuiyanhua@netease.com

[b]College of Chemistry and Materials Engineering, Anhui Science and Technology University, Bengbu 233000, P. R. China

[c]School of Advanced Materials and Nanotechnology, Xidian University, Xi'an 710126, P. R. China. E-mail: zhanghui@xidian.edu.cn

‡ These authors contributed equally to this work.

A typical TFB mainly consists of current collectors, cathode, electrolyte, anode, and packaging layer.[3] In 1982, Hitachi Company first reported an all-solid-state TFB based on TiS$_2$/Li$_{3.6}$Si$_{0.6}$P$_{0.4}$O$_4$/Li, and subsequently NTT Company fabricated a TFB based on LiCoO$_2$/Li$_{3.4}$V$_{0.6}$Si$_{0.4}$O$_4$/Li.[4] However, the electrochemical properties of these TFBs were not satisfactory due to the limitation of the solid electrolyte. Hereafter, Bates *et al.* developed an inorganic solid electrolyte thin film by applying Li$_3$PO$_4$ to a substrate under an N$_2$ atmosphere (LiPON) using a radio frequency (RF) magnetron sputtering approach,[5] which is advantageous because of its high ion conductivity (3.3 $\times$ 10^{-6} S cm^{-1} at 25 °C) and excellent electrochemical stability limit (>5.5 V). Due to its highly stable chemical and electrochemical properties, LiPON has been widely used to fabricate TFBs through integration with high-potential cathodes (such as LiCoO$_2$ and LiMn$_2$O$_4$) and thin film anodes (such as metallic lithium and SnO$_2$).[6–10]

Nonetheless, there are several problems with the LiCoO$_2$–LiPON interface in TFBs based on the LiCoO$_2$/LiPON/Li structure. First, during the discharge process, strain at the electrode–electrolyte interface leads to a significant increase in the internal resistance of the TFBs.[11] Second, the annealing of LiCoO$_2$ thin films generates byproducts (Li$_2$O, CoO, Co$_3$O$_4$), leading to thin film detachment and deterioration of

electrochemical properties.[12] Third, there are severe side reactions between $LiCoO_2$ and LiPON during cycling, which affect the lithium-ion transport at the electrode–electrolyte interface.[13,14] In addition, the formation of disordered $LiCoO_2$ at the $LiCoO_2$/LiPON interface results in lithium accumulation, which leads to further degradation of electrochemical performance.[9]

To reduce the interfacial strain caused by lithium ion extraction/insertion, the occurrence of side reactions must be alleviated, and the wettability and conductivity of the solid–solid interface must be increased. Thus, modification of the $LiCoO_2$–LiPON interface is regarded as a potential method to enhance the electrochemical performance of $LiCoO_2$/LiPON/Li TFBs.[15,16] It was found that a thin protective layer composed of Al_2O_3, MgO, or AlF_3 can assist in eliminating the occurrence of interfacial side reactions.[17–19] However, their poor mechanical and chemical stability limits their widespread applications. In such cases, the elemental interdiffusion and $LiCoO_2$/LiPON space-charge layer between the cathode and electrolyte is effectively suppressed, thereby decreasing the interface resistance and improving the electrochemical performance of TFBs.[20]

For example, Hayashi et al. investigated lithium tungsten oxide-modified $LiCoO_2$ thin film electrodes, which apparently alleviate the hindrance of lithium ion diffusion and increase the frequency factor in $LiCoO_2$, resulting in reduced lithium ion transfer resistance at the interface.[15] The introduction of intercalated pseudocapacitive interface materials for modification of the $LiCoO_2$–LiPON interface is expected to improve its electrochemical performance.

In this work, considering the satisfactory compatibility of amorphous vanadium pentoxide (V_2O_5) with the LiPON interface, we propose to reduce the transfer resistance of lithium ions at the $LiCoO_2$/LiPON interface through the construction of an interfacial nanoscale V_2O_5 buffer layer. There are many unique advantages to amorphous vanadium oxides, such as many defects and active sites, excellent electrochemical stability, and fast ion kinetics.[21,22]

The magnetron sputtering method was used to construct a uniform $LiCoO_2$/V_2O_5/LiPON heterointerface ion conductive network, and its modification and lithium storage mechanism were explored. The scanning electron microscopy (SEM) and energy-dispersive X-ray spectroscopy (EDS) analyses showed that a layer of V_2O_5 was homogeneously coated on the surface of the $LiCoO_2$ cathode. Furthermore, the mechanism behind the lowered resistance with the V_2O_5 modification layer was studied by X-ray photoelectron spectroscopy (XPS) and electrochemical techniques. The XPS analysis confirmed that V_2O_5 interface modification can effectively inhibit undesirable interfacial side reactions. The electrochemical measurements demonstrated that the TFBs based on $LiCoO_2$/V_2O_5/LiPON/Li with a 5 nm-thin V_2O_5 interface modification layer exhibited a high discharge capacity of 34.3 $\mu A\ h\ cm^{-2}\ \mu m^{-1}$ at a current density of 100 $\mu A\ cm^{-2}$ with a capacity retention of 75.6% after 1000 cycles.

2. Experimental section

The fabrication of $LiCoO_2$/V_2O_5/LiPON/Li TFBs with an area of 1 cm^2 was achieved by magnetron sputtering and thermal evaporation using the target/source materials of $LiCoO_2$, V_2O_5, LiPON, and metal Li. Before magnetron sputtering and thermal evaporation deposition, a vacuum was created by evacuating the air in the chamber to 3×10^{-4} Pa for the deposition of each layer. The distance between target material and substrate was set at 7 cm for all the magnetron sputtering procedures. Nine parallel samples were prepared by one magnetron sputtering treatment, which confirmed the satisfactory consistency of TFBs in this work.

2.1. Ti/Pt current collector deposition

The Ti/Pt current collector layer was deposited on a clean glass substrate by direct current (DC) magnetron sputtering. The Ar gas flow rate was adjusted to 100 sccm under a working pressure of 2.0 Pa. The sputtering power was set at 120 W, and the deposition time was 2 minutes. The size of the sputter target was 102.0 mm in diameter and 3 mm in thickness.

2.2. $LiCoO_2$ cathode deposition

The $LiCoO_2$ cathode was deposited on the top of the Ti/Pt layer by RF magnetron sputtering. The Ar and O_2 gas flow rates were adjusted to 80 and 20 sccm, respectively. The working pressure was 2.2 Pa, and the sputtering power was set at 954 W. The deposition time was 30 minutes. The $LiCoO_2$ layer was annealed during deposition at the temperature of 500 °C. The size of the sputter target was 152.4 mm in diameter and 3 mm in thickness.

2.3. V_2O_5 interfacial layer deposition

The V_2O_5 interfacial layer was deposited on the top of the $LiCoO_2$ cathode by RF magnetron sputtering. The Ar and O_2 gas flow rates were adjusted to 70 and 30 sccm, respectively. The working pressure was set at 0.3 Pa, and the sputtering power was 120 W. The deposition time was set at 2–15 minutes. The size of the sputter target was 51.0 mm in diameter and 3 mm in thickness.

2.4. LiPON electrolyte deposition

The LiPON layer was deposited on the top of the V_2O_5 layer (or $LiCoO_2$ cathode layer for parallel samples) by RF magnetron sputtering. The N_2 gas flow rate was adjusted to 100 sccm, and the working pressure was set at 2.0 Pa. The sputtering power was set at 900 W, and the deposition time was 100 minutes.

2.5. Li anode deposition

The Li anode layer was deposited on the top of the LiPON layer in a thermal evaporation system equipped with a glove box. The power was adjusted to 180 W, and the deposition time was 10 minutes.

2.6. Morphological, structural, and electrochemical characterization

The surface morphologies of $LiCoO_2$ and the $LiCoO_2$/V_2O_5 thin films were examined using an SEM apparatus (S-4800, Hitachi). The EDS was acquired by coupling the SEM apparatus with an

EDS component for elemental mapping characterization. The binding energies for $LiCoO_2/V_2O_5/LiPON$ and the $LiCoO_2/LiPON$ thin films were determined by XPS using a PerkinElmer PHI 6000C ECSA system with monochromatic Al K_α (1486.6 eV) irradiation after 20 s of Ar plasma etching at the etch rate of 5 nm min^{-1}.

Cyclic voltammetry (CV) was carried out on a Princeton working station (AMETEK company, PMC CH808A) at a sweep rate of 0.2 mV s^{-1} between 3.0 and 4.2 V. The electrochemical impedance spectra (EIS) were collected at 5 mV AC oscillation amplitude over the frequency range from 10 kHz to 0.01 Hz with an AutoLab PGSTAT302N station. Galvanostatic cycling measurements were carried out with a Land CT2001A battery test system (Wuhan LAND Electronic Co., Ltd), and the cells were cycled in the voltage range from 3.0 to 4.2 V at various current densities.

3. Results and discussion

3.1. Morphological and structural characterization

After deposition of the $LiCoO_2$ cathode film and V_2O_5 interface layer by RF magnetron sputtering, we investigated their surface morphology and elemental distribution. Fig. 1 shows top-view SEM images of $LiCoO_2$ and the V_2O_5 layers of the $LiCoO_2/V_2O_5/LiPON/Li$ all-solid-state TFBs. In Fig. 1a, the surface of the $LiCoO_2$ cathode is uniform, and the film is composed of small particles 20–50 nm in size. Fig. 1b demonstrates that the V_2O_5 interface modification layer is uniform and dense. The EDS mapping of the $LiCoO_2/V_2O_5$ film in Fig. 1c shows that a layer of V_2O_5 was successfully coated on the surface of the $LiCoO_2$ cathode.

We followed the variation of the elemental composition of the films with and without the V_2O_5 interface layer by high-resolution XPS surface analysis. To obtain the interfacial information between the LiPON electrolyte and $LiCoO_2$ cathode in $LiCoO_2/V_2O_5/LiPON$ and $LiCoO_2/LiPON$ films, the LiPON electrolyte was deposited for 10 s, and subsequently used for XPS testing. The binding energies obtained from the XPS analysis were calibrated by referencing the C 1s peak to 284.8 eV. As shown in Fig. 2, the XPS spectra of Li 1s, N 1s, O 1s, and V 2p were obtained in small energy regions around the expected peak positions of each element after layer-by-layer etching of the as-prepared films. Fig. 2a and e show the XPS spectra of Li 1s. The peak at the binding energy of 55.1 eV originated from the Li 1s in $LiCoO_2$. The peak appearing at the binding energy of 56.1 eV was attributed to the Li in LiPON. In addition, there was an additional peak at the binding energy of approximately 54.1 eV, as shown in Fig. 2e, which was attributed to the Li from Li_2O.[23]

For the XPS spectra of N 1s in Fig. 2b and f, the binding energies of 400.1 and 398.4 eV were attributed to the double coordinated nitrogen (N_d) and triple coordinated nitrogen (N_t) in LiPON, respectively.[24] However, the intensity ratio of N_d/N_t in the $LiCoO_2/V_2O_5/LiPON$ film was weaker compared to that in
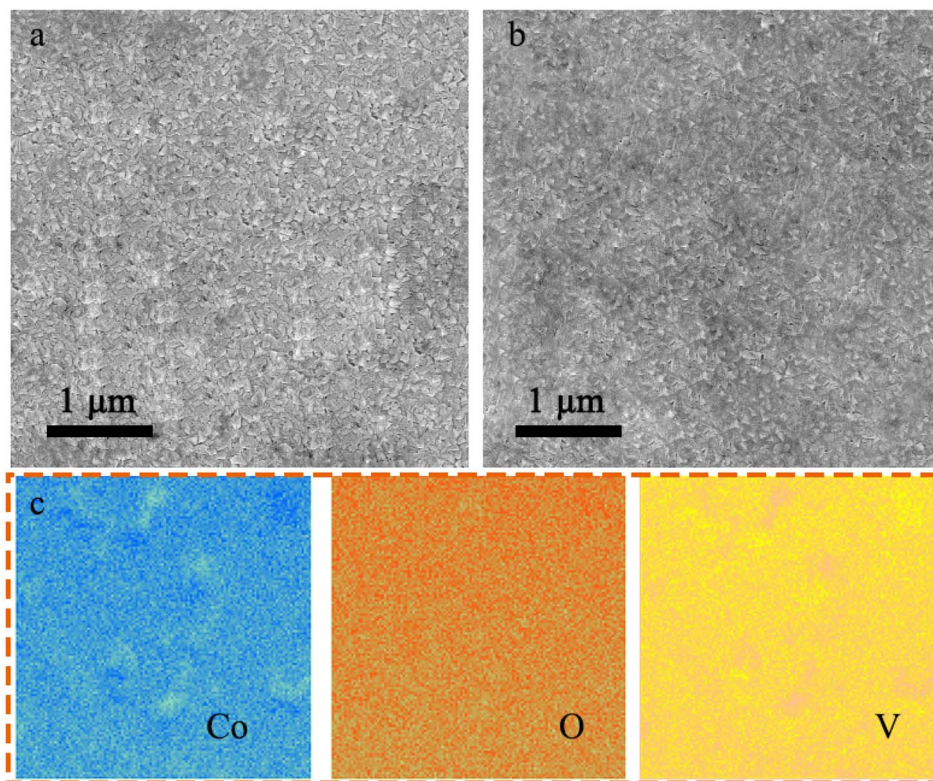

Fig. 1 Representative top-view SEM images for the surface morphology of the as-prepared (a) $LiCoO_2$ cathode film and (b) $LiCoO_2/V_2O_5$ film. (c) The corresponding EDS 2D mapping for element distributions of Co (blue), O (orange), and V (yellow) in the image of (b) the $LiCoO_2/V_2O_5$ film.

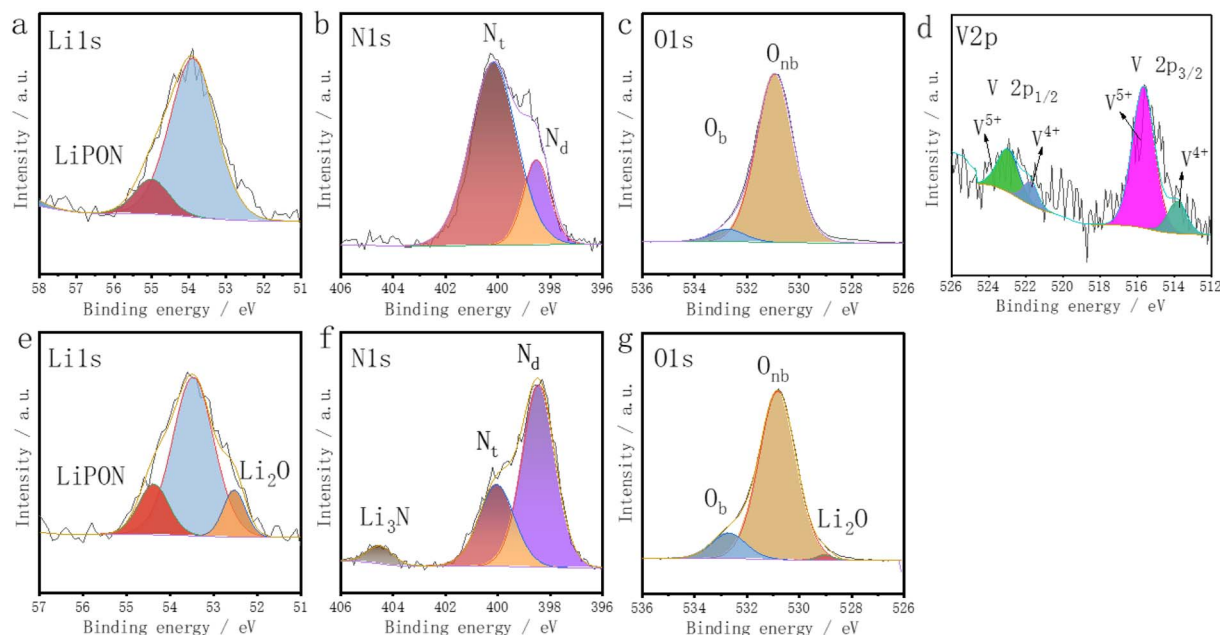Fig. 2 High-resolution XPS spectra for elemental (a) Li 1s, (b) N 1s, (c) O 1s, and (d) V 2p of the LiCoO₂/V₂O₅/LiPON film, and (e) Li 1s (f) N 1s, and (g) O 1s of the LiCoO₂/LiPON film.

the LiCoO$_2$/LiPON film due to the formation of a nitrogen–vanadium triple bond in the former. In Fig. 2f, an additional peak at the binding energy of 404.6 eV appears, which originated from N in Li$_3$N.[25] The XPS spectra of O 1s in Fig. 2c and g show that the binding energies of 533.2 and 531.2 eV were attributed to bridging oxygen (O$_b$) and non-bridging oxygen (O$_{nb}$) in LiPON, respectively. An additional peak in Fig. 2g appears at the binding energy of 529.2 eV, which is the signal of O from Li$_2$O.[26]

Fig. 2d shows the characteristic spectrum of V 2p, which implies the presence of V only in the LiCoO$_2$/V$_2$O$_5$/LiPON film. The de-convoluted XPS spectra of V 2p are given in Fig. 2d, which provides a quantitative idea regarding the valence state of vanadium. The peaks located at 515.7 and 523.0 eV correspond to the V^{5+} 2p$_{3/2}$ and V^{5+} 2p$_{1/2}$ doublet, respectively. Nevertheless, the peaks corresponding to V^{4+} 2p$_{3/2}$ and V^{4+} 2p$_{1/2}$ were also observed at 513.8 and 521.7 eV, respectively. It is worth mentioning that the coexistence of the +4 and +5 oxidation states was significant for increased stability and electronic conductivity, which are crucial for electrochemical application.[27,28] However, in the spectrum of LiCoO$_2$/LiPON, there are no such peaks occurring in same binding energy range.[27]

Fig. S1a† shows the P 2p spectrum of LiPON, which can be resolved into the 2p$_{1/2}$ (131.9 eV), 2p$_{3/2}$ (131.1 eV), and reduced phosphorous (133.0 eV) peaks.[29] The former two peaks were attributed to the phosphorus bonding in PN$_x$O$_{4-x}$ tetrahedrons.[29] Fig. S1b† shows the Co 2p spectrum of LiCoO$_2$, which can be resolved into the 2p$_{1/2}$ peak (794.4 eV), 2p$_{3/2}$ satellite peak (782.6 eV), and 2p$_{3/2}$ peak (788.8 eV).[11] The XPS analysis show that at the interface of LiCoO$_2$/LiPON without V$_2$O$_5$ interface modification, severe side reactions lead to the generation of intermediate and secondary phases, such as Li$_2$O and

Li$_3$N at the interface. XPS analysis confirmed the elemental composition and interface discrepancy in TFBs with or without a V$_2$O$_5$ interface layer, which is consistent with the EDS results. These results demonstrate that V$_2$O$_5$ interface modification can effectively inhibit undesirable interface reactions.

3.2. Electrochemical performance

To investigate the effect of thickness of the V$_2$O$_5$ interface modification layer on the electrochemical performance of TFBs, CV tests were conducted on LiCoO$_2$/V$_2$O$_5$/LiPON/Li TFBs with different thicknesses of the V$_2$O$_5$ interface layer in the voltage range of 3.0–4.2 V at a scan rate of 0.2 mV s^{-1}. Fig. 3 shows the CV curves of TFBs based on the LiCoO$_2$/LiPON/Li and LiCoO$_2$/V$_2$O$_5$/LiPON/Li structure with different thicknesses of V$_2$O$_5$ film, from 2 to 15 nm. The trace trends of CV curves for all the TFBs are similar. The anodic peak occurs in the potential range of 3.9–4.0 V, and the cathodic peak occurs in the potential range of 3.8–3.9 V.

The redox peaks represent two potential stages in the extraction/insertion process of lithium ion transformation in the LiCoO$_2$ structural sites. The redox peaks of V$_2$O$_5$ are located at approximately (3.28 V, 3.12 V) and (3.47 V, 3.34 V).[30] The CV curves in Fig. 3b–e show that there are no significant redox peaks from V$_2$O$_5$ due to the thin V$_2$O$_5$ layer of 2–15 nm, which is much less than that of LiCoO$_2$ layer. The potential differences between the anodic and cathodic peaks are approximately 43, 40, 80, and 159 mV for TFBs based on LiCoO$_2$/V$_2$O$_5$/LiPON/Li with different thicknesses of V$_2$O$_5$ film of 2, 5, 10, and 15 nm, respectively. These results show that the smallest polarization was measured for TFBs with a 5 nm V$_2$O$_5$ layer, as compared to the polarization of TFBs with other thicknesses of interface-modified layers or without a V$_2$O$_5$ layer.
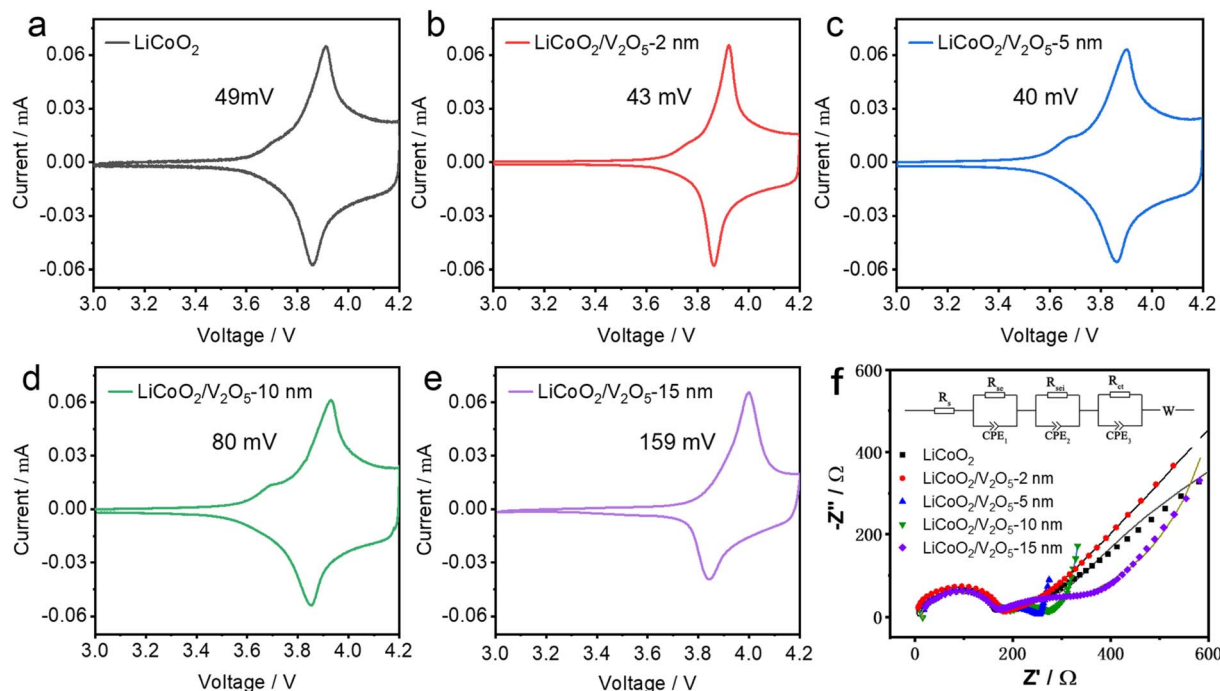

Fig. 3 Cyclic voltammetry of TFBs (a) without V$_2$O$_5$ film or with (b) 2 nm-, (c) 5 nm-, (d) 10 nm-, and (e) 15 nm-thick V$_2$O$_5$ film at a scan rate of 0.2 mV s^{-1} in the potential range of 3.0−4.2 V *versus* metallic Li. (f) Nyquist plots of impedance spectra for TFBs based on LiCoO$_2$/LiPON/Li or LiCoO$_2$/V$_2$O$_5$/LiPON/Li with different thicknesses of V$_2$O$_5$ film at 2, 5, 10, and 15 nm. The fitted results are shown as the solid lines. The inset shows the equivalent circuit used for the analysis of the impedance spectra.

The larger polarization in TFBs based on the LiCoO$_2$/LiPON/Li structure suggests poor reversibility of cycle performance, which could be attributed to the trigger of unrecoverable side reactions between LiCoO$_2$ and the LiPON layers. The larger polarization in TFBs based on the LiCoO$_2$/V$_2$O$_5$/LiPON/Li structure with only a 2 nm thickness for V$_2$O$_5$ may be attributed to insufficient inhibition of side reactions. The larger polarization in TFBs based on the LiCoO$_2$/V$_2$O$_5$/LiPON/Li structure with a greater V$_2$O$_5$ thickness (10 and 15 nm) could be caused by the lower electronic conductivity and ion conductivity of the thick V$_2$O$_5$ modification layer, which can hinder the transfer and diffusion of electrons and ions. These results imply the significantly improved reversibility of the electrochemical lithium ion insertion and extraction process in LiCoO$_2$/V$_2$O$_5$/LiPON/Li with a 5 nm V$_2$O$_5$ layer, which is consistent with the excellent cycling and rate performance of the 5 nm V$_2$O$_5$ layer, as discussed in the following text.

To understand why there was a difference in electrochemical performance between TFBs based on LiCoO$_2$/LiPON/Li and LiCoO$_2$/V$_2$O$_5$/LiPON/Li with different thicknesses of the V$_2$O$_5$ interfacial layer, EIS was employed to analyze the properties of the electrode/electrolyte interface. Fig. 3f shows the EIS spectra of the as-fabricated TFBs before and after V$_2$O$_5$ interfacial modification. The initial intercept of the curve at the Z' axis in the high frequency region represents the ohmic resistance (R_s) of the TFBs. The representative Nyquist plot consists of three semicircles and a diagonal. The semicircle in the high-frequency region represents the impedance of solid electrolyte LiPON (R_{se}). The semicircle in the middle-frequency region represents the solid electrolyte interface (SEI) film impedance (R_{sei}). The semicircle in the low-frequency region is associated with the charge transfer impedance (R_{ct}) at the electrode/electrolyte interface. The diagonal in the low-frequency region was attributed to the Warburg diffusion of lithium ions (Z_w).[31,32]

Table 1 Kinetic parameters of TFBs

TFB	R_{se} (Ω cm^{-2})	R_{sei} (Ω cm^{-2})	R_{ct} (Ω cm^{-2})
LiCoO$_2$/LiPON/Li	142.0	80.8	95.2
LiCoO$_2$/V$_2$O$_5$-2 nm/LiPON/Li	135.7	71.2	85.3
LiCoO$_2$/V$_2$O$_5$-5 nm/LiPON/Li	135.1	62.5	48.6
LiCoO$_2$/V$_2$O$_5$-10 nm/LiPON/Li	133.5	68.4	75.2
LiCoO$_2$/V$_2$O$_5$-15 nm/LiPON/Li	140.9	92.1	163.4

The measured EIS spectra were fitted using an equivalent circuit, as shown in the inset of Fig. 3f, and the fitting results are reported in Table 1.

Table 1 shows that the R_{se} remained similar for all the TFBs, while the R_{ct} and R_{sei} values initially decreased and then increased with the thickness of the V_2O_5 interfacial modification layer. Table 1 shows that the TFBs based on the $LiCoO_2/V_2O_5$-5 nm/LiPON/Li structure exhibited a small R_{ct} value of 48.6 Ω cm^{-2}, which was much less than the value for TFBs without the V_2O_5 layer (95.2 Ω cm^{-2}). This result indicates that the lithium ion diffusion kinetics is enhanced at the electrolyte/electrode interface for TFBs based on the $LiCoO_2/V_2O_5$-5 nm/LiPON/Li structure as compared to TFBs without V_2O_5 layer. However, the TFBs based on the $LiCoO_2/V_2O_5$-15 nm/LiPON/Li structure demonstrate a R_{ct} value of 163.4 Ω cm^{-2}, which is approximately 3.4 times larger than the value of TFBs based on the $LiCoO_2/V_2O_5$-5 nm/LiPON/Li structure.

The V_2O_5 interfacial layer can prevent the direct contact of electrode and electrolyte, which suppresses the side reactions between the $LiCoO_2$ and LiPON layers. The effect may be due to the decomposition products of the SEI, which was also confirmed by XPS measurement in Fig. 2. As a result, the V_2O_5 thin film can enhance the diffusion kinetics of lithium ions and reduce the interface resistance. However, if the thickness of the modification layer is too great, electron and ion transfer and diffusion will be inhibited. This results in an increase in the interface resistance when the thickness of the V_2O_5 layer is greater than 5 nm, which would decrease the electrochemical lithium ion storage performance with further increasing thickness of the V_2O_5 layer. The EIS results imply that the electrochemical performance in TFBs based on $LiCoO_2/V_2O_5$-5 nm/LiPON/Li would be significantly enhanced as compared to that in TFBs without a V_2O_5 layer, while a larger impedance in TFBs based on $LiCoO_2/V_2O_5$-15 nm/LiPON/Li would exacerbate their decay capacity.

Fig. 4a and b shows the cyclic stability and rate performance of TFBs based on the $LiCoO_2$/LiPON/Li structure and $LiCoO_2$/V_2O_5/LiPON/Li structure with different thicknesses of the V_2O_5 modification layers in the potential range of 3.0–4.2 V. The discharge capacities of TFBs based on $LiCoO_2$/LiPON/Li, $LiCoO_2/V_2O_5$-2 nm/LiPON/Li, $LiCoO_2/V_2O_5$-5 nm/LiPON/Li, $LiCoO_2/V_2O_5$-10 nm/LiPON/Li, and $LiCoO_2/V_2O_5$-15 nm/LiPON/Li can be maintained at 31.9, 33.2, 34.3, 31.8, and 30.7 μA h cm^{-2} μm^{-1} after 1000 cycles, respectively. The coulombic efficiency stabilizes at more than 95% for all the samples. The average discharge capacities of TFBs based on $LiCoO_2/V_2O_5$-5 nm/LiPON/Li are approximately 40.5, 39.7, 39.3, 38.9, 38.6, and 39.7 μA h cm^{-2} μm^{-1} at discharge current densities of 20, 40,

Fig. 4 Electrochemical properties for TFBs based on $LiCoO_2$/LiPON/Li or $LiCoO_2$/V_2O_5/LiPON/Li with different thicknesses of the V_2O_5 modification layers. (a) Cycling behaviors and coulombic efficiency at a current density of 100 μA cm^{-2} in the potential range of 3.0–4.2 V *versus* metallic Li. (b) Rate performance at different current densities of 20, 40, 60, 80, 100, and 20 μA cm^{-2}, respectively. The differential capacity (dQ/dV) *versus* voltage derived from the 2nd and 1000th charge–discharge curves of TFBs based on the (c) $LiCoO_2$/LiPON/Li and (d) $LiCoO_2$/V_2O_5-5 nm/LiPON/Li structures.

Fig. 6 The variation of impedance (a) R_{se}, (b) R_{sei}, and (c) R_{ct} with different charge–discharge states (depth of charge, doc) from 0% to 100% at the interval of 10% for all-solid-state TFBs based on $LiCoO_2/LiPON/Li$ and $LiCoO_2/V_2O_5$-5 nm/LiPON/Li.

4. Conclusion

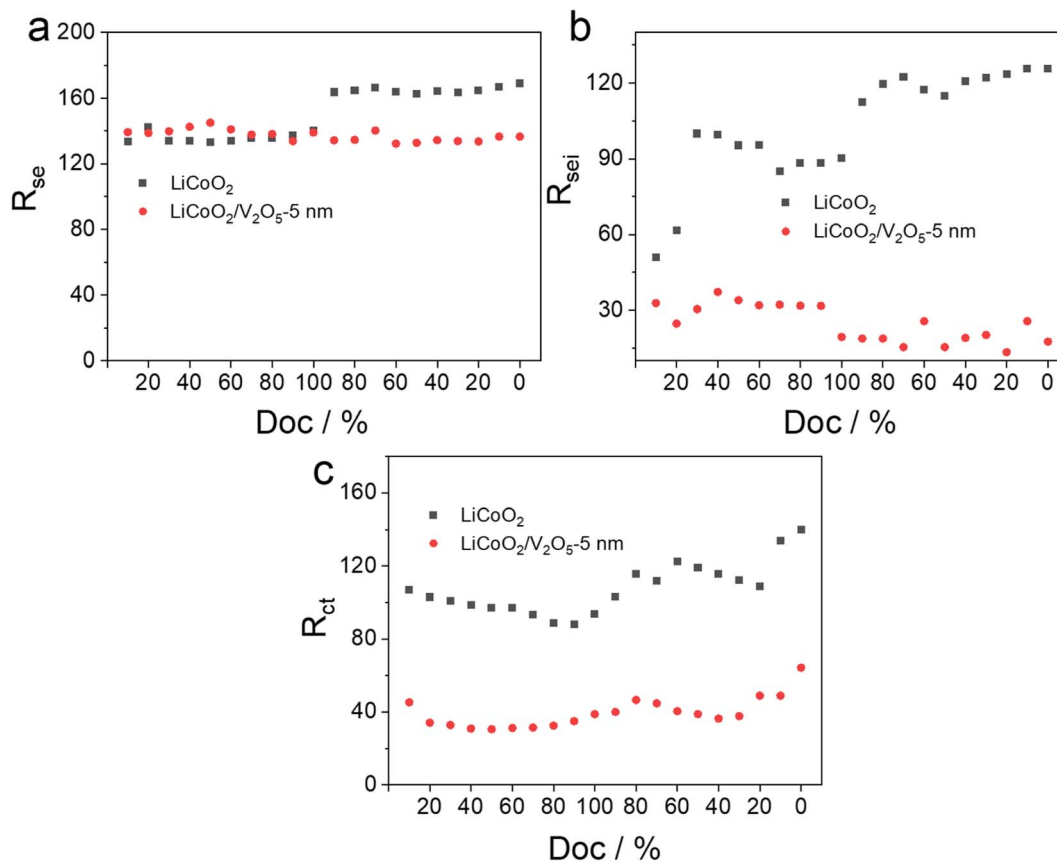In this work, a V_2O_5 thin film layer was introduced at the $LiCoO_2/LiPON$ heterojunction interface to improve the interfacial transport dynamics of TFBs *via* a magnetron sputtering method. The V_2O_5 thin film layer at the heterogeneous interface assisted in constructing an ion transport network, which reduced the electrochemical redox polarization potential from 49 mV to 40 mV. The V_2O_5 interfacial layer effectively suppressed the side reactions between $LiCoO_2$ and LiPON. After 1000 cycles, the electrochemical polarization potential increased by only approximately 2 mV, indicating the more stable interface between electrode and electrolyte in TFBs based on $LiCoO_2/V_2O_5$-5 nm/LiPON/Li.

It was found that the thickness of the V_2O_5 modification layers significantly influenced the performance of $LiCoO_2/V_2O_5/LiPON/Li$ all-solid-state TFBs. The TFBs based on $LiCoO_2/V_2O_5/LiPON/Li$ with a 5 nm V_2O_5 thin layer showed the smallest R_{ct} value of 48.6 $\Omega\ cm^{-2}$, which is only approximately half of the R_{ct} value for TFBs without the V_2O_5 modification layer (95.2 $\Omega\ cm^{-2}$). As a result, the TFBs based on $LiCoO_2/V_2O_5$-5 nm/LiPON/Li exhibited a significantly increased discharge specific capacity, and superior cycling and rate performance, which was much higher than that of TFBs without the V_2O_5 modification layer. The discharge capacity remained at 75.6% of its initial value after 1000 cycles at a current

density of 100 μA cm^{-2}. This was mainly attributed to the enhanced lithium ion transport kinetics and the suppression of severe side reactions at the cathode–electrolyte interface in TFBs based on $LiCoO_2/V_2O_5/LiPON/Li$ with a 5 nm V_2O_5 thin layer, thereby achieving satisfactory electrochemical performance. This study provides an in-depth understanding of the mechanism governing electrochemical performance degradation in $LiCoO_2/LiPON/Li$ TFBs, and also demonstrates an efficient approach to improve the electrochemical performance of TFBs through V_2O_5 interface layer engineering.

Conflicts of interest

There are no conflicts to declare.

Acknowledgements

References

1 J. Lin, L. Lin, S. Qu, D. Deng, Y. Wu, X. Yan, Q. Xie, L. Wang and D. Peng, *Energy Environ. Mater.*, 2022, **5**, 133–156.

2 T. Wu, W. Dai, M. Ke, Q. Huang and L. Lu, *Adv. Sci.*, 2021, **8**, 2100774.

3 T. Wu, Y. Zhao, X. Zhang, S. Ma, K. Wei, Y. Wei and Y. Cui, *Appl. Surf. Sci.*, 2022, **591**, 153174.

4 K. Kanehori, K. Matsumoto, K. Miyauchi and T. Kudo, *Solid State Ionics*, 1983, **9–10**, 1445–1448.

5 J. B. Bates, N. J. Dudney, G. R. Gruzalski, R. A. Zuhr, A. Choudry, C. F. Luck and J. D. Robertson, *Solid State Ionics*, 1992, **53**, 647–654.

6 C. Santoro, C. Arbizzani, B. Erable and I. Ieropoulos, *J. Power Sources*, 2017, **356**, 225–244.

7 Q. Xia, Q. Zhang, S. Sun, F. Hussain, C. Zhang, X. Zhu, F. Meng, K. Liu, H. Geng, J. Xu, F. Zan, P. Wang, L. Gu and H. Xia, *Adv. Mater.*, 2021, **33**, 2003524.

8 J. Lin, J. Guo, C. Liu and H. Guo, *ACS Appl. Mater. Interfaces*, 2016, **8**, 34372–34378.

9 Z. Wang, J. Z. Lee, H. L. Xin, L. Han, N. Grillon, D. Guy-Bouyssou, E. Bouyssou, M. Proust and Y. S. Meng, *J. Power Sources*, 2016, **324**, 342–348.

10 L. Li, S. Liu, H. Zhou, Q. Lei and K. Qian, *Mater. Lett.*, 2018, **216**, 135–138.

11 S. S. Qu, W. B. Wu, Y. F. Wu, Y. P. Zhuang, J. Lin, L. S. Wang, Q. L. Wei, Q. S. Xie and D. L. Peng, *Nanomaterials*, 2021, **11**, 3393.

12 L. Yang, X. Li, K. Pei, W. You, X. Liu, H. Xia, Y. Wang and R. Che, *Adv. Funct. Mater.*, 2021, **31**, 2103971.

13 K. Leung, A. J. Pearse, A. A. Talin, E. J. Fuller, G. W. Rubloff and N. A. Modine, *ChemSusChem*, 2018, **11**, 1956–1969.

14 D. Santhanagopalan, D. Qian, T. McGilvray, Z. Wang, F. Wang, F. Camino, J. Graetz, N. Dudney and Y. S. Meng, *Energy Environ. Mater.*, 2014, **5**, 298–303.

15 T. Hayashi, J. Okada, E. Toda, R. Kuzuo, Y. Matsuda, N. Kuwata and J. Kawamura, *J. Power Sources*, 2015, **285**, 559–567.

16 T. Marukame, K. Mizushima, K. Nomura and Y. Nishi, *IEEE J. Electron Devices Soc.*, 2023, **11**, 602–610.

17 S. U. Woo, C. S. Yoon, K. Amine, I. Belharouak and Y. K. Sun, *J. Electrochem. Soc.*, 2007, **154**, A1005.

18 A. Zhou, Q. Liu, Y. Wang, W. Wang, X. Yao, W. Hu, L. Zhang, X. Yu, J. Li and H. Li, *J. Mater. Chem. A*, 2017, **5**, 24361–24370.

19 Y. Orikasa, D. Takamatsu, K. Yamamoto, Y. Koyama, S. Mori, T. Masese, T. Mori, T. Minato, H. Tanida, T. Uruga, Z. Ogumi and Y. Uchimoto, *Adv. Mater. Interfaces*, 2014, **1**, 1400195.

20 M. Fingerle, R. Buchheit, S. Sicolo, K. Albe and R. Hausbrand, *Chem. Mater.*, 2017, **29**, 7675–7685.

21 F. Mattelaer, K. Geryl, G. Rampelberg, J. Dendooven and C. Detavernier, *ACS Appl. Mater. Interfaces*, 2017, **9**, 13121–13131.

22 Q. He, Z. Chen, X. Niu, X. Han, T. Kang, J. Chen, Y. Ma and J. Zhao, *Nano Res.*, 2023, **16**, 9195–9213.

23 G. Cherkashinin, Z. Yu, R. Eilhardt, L. Alff and W. Jaegermann, *Adv. Mater. Interfaces*, 2020, **7**, 2000276.

24 J. Ko and Y. S. Yoon, *Ceram. Int.*, 2020, **46**, 20623–20632.

25 A. Schwoebel, R. Hausbrand and W. Jaegermann, *Solid State Ionics*, 2015, **273**, 51–54.

26 D.-J. Yun, S. Lim, J. Y. Won, K. Kim, H. Lee, J. Hwang, J. Chung, Y. S. Kim, Y.-N. Kwon, E. Lee, J. Baik and W.-Y. Yang, *J. Power Sources*, 2018, **399**, 231–237.

27 M. Ghosh, V. Vijayakumar, R. Soni and S. Kurungot, *Nanoscale*, 2018, **10**, 8741–8751.

28 F. Mattelaer, K. Geryl, G. Rampelberg, T. Dobbelaere, J. Dendooven and C. Detavernier, *RSC Adv.*, 2016, **6**, 114658–114665.

29 S. Zhou, R. Tian, A. Wu, L. Lin and H. Huang, *J. Energy Chem.*, 2022, **75**, 349–359.

30 Q. An, P. Zhang, F. Xiong, Q. Wei, J. Sheng, Q. Wang and L. Mai, *Nano Res.*, 2015, **8**, 481–490.

31 S. Larfaillou, D. Guy-Bouyssou, F. le Cras and S. Franger, *J. Power Sources*, 2016, **319**, 139–146.

32 Y. Iriyama, T. Kako, C. Yada, T. Abe and Z. Ogumi, *Solid State Ionics*, 2005, **176**, 2371–2376.

33 J. N. Reimers and J. R. Dahn, *J. Electrochem. Soc.*, 1992, **139**, 2091.